Porcine deltacoronavirus accessory protein NS6 antagonizes IFN-β production by interfering with the binding of RIG-I/MDA5 to double-stranded RNA

Puxian Fang[a,b], Liurong Fang[a,b], Jie Ren[a,b], Yingying Hong[a,b], Xiaorong Liu[a,b], Yunyang Zhao[a,b], Dang Wang[a,b], Guiqing Peng[a,b], and Shaobo Xiao[a,b#]

[a]State Key Laboratory of Agricultural Microbiology, College of Veterinary Medicine, Huazhong Agricultural University, Wuhan 430070, China

[b]The Key Laboratory of Preventive Veterinary Medicine in Hubei Province, Cooperative Innovation Center for Sustainable Pig Production, Wuhan 430070, China

[#]Corresponding author. Laboratory of Animal Virology, College of Veterinary Medicine, Huazhong Agricultural University, 1 Shi-zi-shan Street, Wuhan 430070, China. E-mails: vet@mail.hzau.edu.cn

Running title: *PDCoV NS6 antagonizes IFN-β production*

Abstract word count: 229

Main text word count: 5299

ABSTRACT

Porcine deltacoronavirus (PDCoV) has recently emerged as an enteric pathogen that can cause serious vomiting and diarrhea in suckling piglets. The first outbreak of PDCoV occurred in the United States in 2014 and was followed by reports of PDCoV in South Korea, China, Thailand, Lao people's Democratic Republic, and Vietnam, leading to economic losses for pig farms and posing considerable threat to the swine industry worldwide. Our previous studies have shown that PDCoV encodes three accessory proteins, NS6, NS7, and NS7a, but the functions of these proteins in viral replication, pathogenesis, and immune regulation remain unclear. Here, we found that ectopic expression of accessory protein NS6 significantly inhibits Sendai virus-induced interferon-β (IFN-β) production, as well as the activation of transcription factors IRF3 and NF-κB. Interestingly, NS6 does not impede the IFN-β promoter activation mediated via key molecules in the RIG-I-like receptor (RLR) signaling pathway, specifically RIG-I, MDA5, and their downstream molecules MAVS, TBK1, IKKε, and IRF3. Further analyses revealed that NS6 is not a RNA-binding protein; however, it interacts with RIG-I/MDA5. This interaction attenuates the binding of double-stranded RNA by RIG-I/MDA5, resulting in the reduction of RLR-mediated IFN-β production. Taken together, our results demonstrate that ectopic expression of NS6 antagonizes IFN-β production by interfering with the binding of RIG-I/MDA5 to double-stranded RNA, revealing a new strategy employed by PDCoV accessory proteins to counteract the host innate antiviral immune response.

42 **IMPORTANCE**

43 Coronavirus accessory proteins are species-specific, and they perform multiple
44 functions in viral pathogenicity and immunity, such as acting as interferon (IFN)
45 antagonists and cell death inducers. Our previous studies have shown that porcine
46 deltacoronavirus (PDCoV) encodes three accessory proteins. Here, we demonstrated
47 for the first time that PDCoV accessory protein NS6 antagonizes IFN-β production by
48 interacting with RIG-I and MDA5 to impede their association with double-stranded
49 RNA. This is an efficient strategy of antagonizing type I IFN production by disrupting
50 the binding of host pattern recognition receptors (PRRs) and pathogen-associated
51 molecular patterns (PAMPs). These findings deepen our understanding of the function
52 of accessory protein NS6 and may direct us toward novel therapeutic targets and lead
53 to the development of more effective vaccines against PDCoV infection.

INTRODUCTION

Porcine deltacoronavirus (PDCoV) is a swine enteropathogenic coronavirus that can lead to acute diarrhea and vomiting in infected nursing piglets (1-3). PDCoV was first detected in Hong Kong in 2012 (4). However, the first outbreak of PDCoV occurred in Ohio in 2014, after which it rapidly spread to other states of the United States (5-9). Subsequently, other countries, including South Korea (10), China (11-13), Thailand (14), Lao people's Democratic Republic (15), and Vietnam (16) have reported a prevalence of PDCoV. Furthermore, a recent report indicated that calves are also susceptible to PDCoV, highlighting the significant threat to animal health posed by this virus and gaining tremendous attention (17, 18).

PDCoV is an enveloped, single-stranded, positive-sense RNA virus belonging to the genus *Deltacoronavirus* of the family Coronaviridae (4). The full-length genome of PDCoV is approximately 25.4 kb in length, with the essential genes occurring in the order 5′ UTR-ORF1a/1b-S-E-M-NS6-N-NS7-NS7a-3′ UTR and encoding a total of 15 mature nonstructural proteins, four structural proteins, and three accessory proteins (13, 19-21). Coronavirus accessory proteins are species-specific, and each coronavirus encodes various amounts of accessory proteins interspaced between viral structural protein genes. For example, feline infectious peritonitis virus (FIPV), which is an alphacoronavirus, and infectious bronchitis virus (IBV), which is a gammacoronavirus, each have four accessory proteins, while another alphacoronavirus, porcine epidemic diarrhea virus (PEDV), has only one accessory protein and the betacoronavirus severe acute respiratory syndrome coronavirus

(SARS-CoV) has eight (22). Though coronavirus accessory proteins have been widely considered to be dispensable for viral replication *in vitro* (23-25), extensive reports have indicated that many accessory proteins are involved in immune regulation, such as SARS-CoV ORF3b, ORF6, and ORF9b (26-28), the Middle East respiratory syndrome coronavirus (MERS-CoV) ORF4a and ORF4b (29-31), and mouse hepatitis virus (MHV) ns2 (32, 33). To our knowledge, there is no report on the functions of PDCoV accessory proteins.

In virus-infected cells, certain viral RNA replication intermediates, leader RNAs, or defective interfering RNAs with 5′ triphosphates are generated, and these substances act as pathogen-associated molecular patterns (PAMPs) that are recognized by host pattern-recognition receptors (PRRs), such as retinoic acid-induced gene I (RIG-I) and melanoma differentiation gene 5 (MDA5) in the cytoplasm (34-36). Upon PAMP recognition, RIG-I and MDA5 are activated, resulting in the recruitment of mitochondrial antiviral signaling protein (MAVS) (also known as IPS-1, VIAS, or Cardif) to the RIG-I-like receptor (RLR) signalosome; this leads to IFN-β production via activation of the complex formed by transcription factor IRF3 and NF-κB-activator TBK1/IKKε followed by the subsequent activation of IRF3 and NF-κB (37, 38). However, many viruses, including CoVs, have evolved various mechanisms to antagonize IFN via targeting multiple steps in the IFN signaling pathway (39-44). Previous studies have demonstrated that PDCoV infection suppresses the RIG-I-mediated production of type I IFN (45). However, the details of the molecular mechanism by which PDCoV regulates IFN activity are still largely

98 unknown. Accessory protein NS6 is encoded between the M and N genes in the
99 PDCoV genome; it is expressed in virus-infected cytoplasm and has been detected in
100 purified virions (19). Interestingly, SARS-CoV accessory proteins ORF6 and ORF9b
101 have also been identified as virion-associated proteins, as well as IFN antagonists
102 (46-48). Therefore, we are aimed to investigate whether or not PDCoV NS6
103 participates in the regulation of the RLR-mediated IFN signaling pathway.

104 In this study, our findings clearly reveal that overexpression of PDCoV NS6
105 inhibits IFN-β production via interacting with RIG-I and MDA5 to disturb their
106 association with PAMP double-stranded RNA (dsRNA), a known initial step of IFN
107 signaling pathway.

108

109 **RESULTS**

110 **PDCoV NS6 inhibits Sendai virus (SeV)-induced IFN-β production**

111 To investigate whether or not PDCoV NS6 is an IFN antagonist, human embryonic
112 kidney (HEK-293T) cells or porcine kidney (LLC-PK1) cells were co-transfected for
113 24 h with increasing amounts of NS6 expression plasmid (pCAGGS-HA-NS6) or
114 empty vector, together with the firefly luciferase reporter plasmid IFN-β-Luc and
115 *Renilla* luciferase reporter plasmid pRL-TK (as internal control), and then infected
116 with SeV for 12 h. The cells were lysed, and the resultant lysates were subjected to
117 dual-luciferase reporter assays. The results showed that the SeV-induced IFN-β-Luc
118 promoter activation was significantly inhibited by NS6 overexpression in both cell
119 lines (**Fig. 1A and 1B**). To further confirm the results from these IFN-β-Luc reporter

assays, we performed IFN bioassays by using an IFN-sensitive vesicular stomatitis virus expressing green fluorescent protein (VSV-GFP). The level of VSV-GFP replication is inversely linked to the levels of secreted IFN-α/β from the transfected HEK-293T cells. As seen in **Fig. 1C**, cellular supernatants from SeV-infected cells significantly inhibited the replication of VSV-GFP in HEK-293T cells. However, the natural replication of VSV-GFP was, to a large extent, restored by the presence of supernatants from cells expressing NS6 compared with that of supernatants from empty vector-transfected cells. To rule out the possibility that the NS6 protein itself affects the replication of SeV, relatively quantitative real-time RT-PCR was performed to detect SeV HN gene expression in pCAGGS-HA–NS6-transfected HEK-293T cells. As shown in **Fig. 1D**, there was no significant difference in the amount of SeV HN mRNA in pCAGGS-HA-NS6-transfected cells compared with that in empty vector-transfected cells, indicating that the observed NS6-mediated inhibition of IFN expression was not due to a general restriction of SeV replication. These results strongly indicate that PDCoV NS6 antagonizes IFN-β production.

PDCoV NS6 impairs activation of IRF3 and NF-κB

The transcription factors IRF3 and NF-κB are required for the induction of IFN-β production. Since our above results indicate that PDCoV NS6 antagonizes IFN-β production, we next explored the effect of NS6 on the activation of IRF3 and NF-κB. To this end, HEK-293T cells were transfected with pCAGGS-HA-NS6 and the luciferase reporter plasmid IRF3-Luc or NF-κB-Luc (each contains four copies of the

IRF- or NF-κB-binding motif of the IFN-β promoter upstream of the firefly luciferase reporter gene), along with the internal control plasmid pRL-TK, followed 24 h later by stimulation with SeV for 12 h. As seen in **Fig. 2**, the SeV-induced activation of both IRF3-dependent (**Fig.2A**) and NF-κB-dependent (**Fig.2B**) promoters was dose-dependently impaired by overexpressing NS6.

IRF3 and NF-κB are regarded as critical regulatory factors in the initiation of the innate antiviral response. They are activated via phosphorylation and nuclear translocation upon viral infection, followed by the assembly of coordinately activated transcription factors and the induction of transcription of specific defense genes, such as IFN-β (49, 50). Therefore, we further investigated the impact of NS6 protein on the phosphorylation and nuclear translocation of IRF3 and NF-κB by performing western blotting and indirect immunofluorescent assays (IFAs). As shown in **Fig. 2**, the levels of phosphorylated IRF3 and p65 were markedly enhanced in SeV-infected cells compared with those in mock-infected cells. However, the SeV-mediated IRF3 and p65 phosphorylation levels were notably lower in NS6-expressing cells (**Fig. 2C and 2D**). In agreement with the western blot results, the nuclear translocations of IRF3 and p65 were also impeded by NS6 protein (**Fig. 2E and 2F**). These results strongly support the idea that PDCoV NS6 acts as an IFN antagonistic protein by blocking the activation of IRF3 and p65.

PDCoV NS6 fails to disrupt IFN-β promoter activation driven by RIG-I, MDA5, MAVS, TBK1, IKKε, or IRF3

SeV is a strong inducer of the RLR-mediated IFN-β signaling pathway (51). The finding that NS6 protein inhibits the SeV-mediated activation of IRF3 and p65 indicates that NS6 protein may block the RLR-mediated type I IFN signaling pathway. To investigate this possibility and to determine at which step the NS6 protein displays its activity, we measured the effect of NS6 on the IFN-β production induced by a series of key signaling molecules in the RLR signaling pathway, specifically RIG-I, RIG-IN (a constitutively activated RIG-I mutant), MDA5, MAVS, TBK1, IKKε, and IRF3. Based on a comparison with the corresponding empty vector-transfected cells, NS6 failed to block the activation of the IFN-β promoter in cells overexpressing any of the above signaling molecules (**Fig. 3**). These results suggest that the inhibition of IFN-β production by NS6 may occur via targeting the RLR signaling pathway at the level of RIG-I/MDA5 or the upstream signaling components.

NS6 protein blocks the IFN-β promoter activation induced by the combination of RIG-I/MDA5 and SeV/poly(I:C)

Although NS6 does not inhibit RIG-I/MDA5-mediated IFN-β promoter activation (**Fig. 3A and 3B**), the ectopic expression of NS6 significantly inhibits SeV-mediated IFN-β production (**Fig. 1A and 1B**). To further investigate the role of NS6, we next examined the effect of NS6 on the SeV-induced IFN-β promoter activation in RIG-I- or MDA5-expressing cells. HEK-293T cell were transfected with an expression construct encoding full-length RIG-I or MDA5 or with an empty vector, along with pCAGGS-HA-NS6 or its corresponding empty vector. After 24 h, these cells were

186 stimulated with SeV or poly(I:C) (a synthetic mimic of dsRNA) for 12 h, after which
187 dual-luciferase reporter assays were performed. As shown in **Fig. 4**, SeV/poly(I:C)
188 stimulation notably induced the activation of the IFN-β promoter, but the increased
189 activation was significantly lower in the presence of NS6 protein. Overexpression of
190 either RIG-I or MDA5 resulted in a significant activation of IFN-β promoter, and this
191 activation did not appear to be inhibited by NS6 protein. These results are consistent
192 with those shown in Fig. 1A and Fig. 3A and 3B. RIG-I/MDA5-mediated activation of
193 the IFN-β promoter increased dramatically following stimulation with SeV or
194 poly(I:C). However, the synergistic activation of IFN-β promoter induced by RIG-I
195 **(Fig. 4A and 4B)** or MDA5 **(Fig. 4C and 4D)** coupled with SeV/poly(I:C) was
196 significantly inhibited by NS6 protein. Based on these findings, we speculate that the
197 inhibition of IFN-β production by NS6 may occur at the
198 RIG-I/MDA5-dsRNA-recognition step.
199
200 **NS6 protein interacts with both RIG-I and MDA5**
201 To further investigate the hypothesis that NS6 targets the initial
202 RIG-I/MDA5-dsRNA-recognition step, we tested if NS6 is able to interact with RIG-I
203 or MDA5, leading to the blockage of their functions. HEK-293T cells were
204 co-transfected with expression plasmids encoding HA-tagged NS6 protein and
205 Flag-tagged RIG-I or MDA5, followed by co-immunoprecipitation (Co-IP) and
206 western blot analyses with anti-HA and anti-Flag monoclonal antibodies (MAbs),
207 respectively. Both RIG-I and MDA5 were efficiently co-immunoprecipitated with

208 HA-NS6 by anti-HA MAb (**Fig. 5A and 5B**). In a reverse Co-IP experiment, NS6
209 proteins were also efficiently co-immunoprecipitated with RIG-I or MDA5 by
210 anti-Flag MAb (**Fig. 5C and 5D**). Furthermore, IFAs also demonstrated that HA-NS6
211 and Flag-RIG-I or MDA5 were co-localized and were both distributed predominately
212 in the cytoplasm (**Fig. 5E and 5F)**.

213 Previous studies have identified RIG-I and MDA5 as dsRNA-binding proteins
214 (29, 52). Based on this feature, we hypothesized that the interaction between NS6 and
215 RIG-I or MDA5 may be mediated by RNA with a tertiary complex form. To test this
216 possibility, HEK-293T cells were co-transfected with NS6 and RIG-I or MDA5
217 expression plasmids for 24 h, followed by the transfection with poly(I:C). To exclude
218 the non-specific binding of NS6 with RIG-I or MDA5, cells co-transfected with
219 plasmid encoding green fluorescent protein (GFP) were used as control. The lysates
220 from transfected cells were treated with RNase A (50 μg/ml, TaKaRa) and then
221 subjected to immunoprecipitation with anti-HA (IP: HA). As shown in **Fig. 5G and**
222 **5H**, both RIG-I and MDA5, but not GFP, could be co-immunoprecipitated with NS6
223 protein under RNase A treatment, and the Co-IP efficiency did not change by the
224 addition of RNase A. These results indicate that the specific interaction between
225 RIG-I or MDA5 and NS6 is RNA-independent.

226

227 **NS6 interacts with the carboxyl terminus domain of RIG-I and the helicase and**
228 **carboxyl terminus domains of MDA5**

229 Both RIG-I and MDA5 are RIG-I-like receptors, and they harbor similar functional

domains for the activation of type I IFN, including two N-terminal caspase-recruitment (CARDs) domains, a central DExD/H-box helicase domain (Hel), and a C-terminal domain (CTD) (53). To explore which domain of RIG-I/MDA5 binds to NS6, various expression plasmids encoding the 2CARD, Hel, or CTD of RIG-I/MDA5, were constructed. HEK-293T cells were co-transfected with HA-NS6 and a Flag-tagged 2CARD, Hel, or CTD expression plasmid of RIG-I/MDA5. At 28 h post-transfection, the cells were harvested and subjected to Co-IP analyses with anti-HA or anti-Flag MAb. When the immunoprecipitation was performed with anti-HA MAb, NS6 co-immunoprecipitated with the CTD of RIG-I, or the Hel and CTD of MDA5, but not with other mutants of RIG-I/MDA5 (**Fig. 6A and B**). In the reverse Co-IP experiments with anti-Flag MAb, both RIG-I CTD and MDA5 Hel and CTD were able to co-immunoprecipitate with NS6 (**Fig. 6C and D**). Together, these results indicate that NS6 specifically interacts with the CTD of RIG-I and the Hel and CTD of MDA5

NS6 is not a dsRNA-binding protein

To investigate whether or not NS6 protein is able to bind RNA molecules, we performed a pulldown experiment with poly(I:C)-coated agarose beads or poly(C)-coated agarose beads (Sigma) (as negative control). This method has been extensively used to identify viral RNA-binding proteins, such as MERS-CoV 4a and Ebola VP35 protein (29, 54). RIG-I served as a positive control because it has been proven to interact directly with poly(I:C) (52). Previous work demonstrated that the

252 binding of N protein to RNA is a widespread feature for coronaviruses (55), so we
253 investigated whether or not PDCoV N protein has a similar characteristic. As shown
254 in **Fig. 7**, RIG-I could be detected bound to poly(I:C)-coated agarose beads but not
255 bound to poly(C)-coated agarose beads, further confirming that RIG-I binds dsRNA;
256 PDCoV N protein was found bound to both poly(I:C)-coated agarose beads and
257 poly(C)-coated agarose beads, indicating that PDCoV N protein can bind both double-
258 and single-stranded RNA. However, NS6 protein was not detected bound to either
259 poly(I:C)-coated agarose beads or poly(C)-coated agarose beads, verifying that NS6 is
260 not a RNA-binding protein.
261
262 **NS6 attenuates the interaction of dsRNA with RIG-I/MDA5**
263 Given our above finding that NS6 is not a RNA-binding protein, the possibility that
264 NS6 inhibits SeV/poly(I:C)-induced IFN-β production by competing with
265 RIG-I/MDA5 for dsRNA binding can be excluded. Thus, we speculated that NS6
266 protein disrupts or attenuates the binding of dsRNA with RIG-I/MDA5. A competition
267 assay was performed by using a poly(I:C) pulldown assay. HEK-293T cells were
268 transfected with Flag-RIG-I or -MDA5 and increasing amounts of HA-NS6. The
269 clarified lysates from cells transfected with RIG-I or MDA5 expression constructs
270 were incubated with those from cells transfected with increasing concentrations of
271 NS6 expression plasmid, followed by supplementation with prepared poly(I:C)-coated
272 agarose beads for 4 h at 4 °C. Bound RIG-I or MDA5 was then detected by western
273 blotting. As seen in **Fig. 8**, the expressions of RIG-I, MDA5, and NS6 proteins were

clearly detected in whole cell lysates; however, significantly lower amounts of RIG-I (**Fig. 8A**) and MDA5 (**Fig. 8B**) co-immunoprecipitated with poly(I:C)-coated agarose beads were detected with increasing concentrations of NS6 protein. These results indicate that NS6 protein at least partially functions to block the recognition or binding of dsRNA by RIG-I or MDA5, leading to the antagonism of IFN-β production.

DISCUSSION

As species-specific proteins of coronaviruses, accessory proteins have received increasingly more attention over the past decade, and novel accessory proteins encoded by coronaviruses have been continually identified in virus-infected cells, such as the ORFX of bat SARS-like coronavirus (56) and the NS7a protein of PDCoV (20). In this study, we investigated the function of PDCoV NS6. Our results reveal that NS6 possesses the property of antagonizing IFN-β production, and it does so by interacting with the CTD of RIG-I and the Hel and CTD of MDA5, which attenuates the binding of RIG-I/MDA5-dsRNA.

RIG-I and MDA5 belong to the RIG-I-like helicase group of the SF2 family, and they are important cytoplasmic PRRs, which function as viral dsRNA receptors to initiate the type I IFN response against infection with an RNA virus (57). For CoV, MDA5 appears to be more important than RIG-I to recognize CoV replicative intermediates (58, 59). In an effort to evade host immune surveillance, many viral proteins target these two molecules to disrupt IFN signaling. For example, both

296 human respiratory syncytial virus NS2 protein and New World Arenavirus Z protein
297 antagonize the activation of IFN-β production via interacting with RIG-I to disturb its
298 association with the downstream signaling molecule MAVS (60, 61). Additionally, the
299 X protein encoded by Hepatitis B virus suppresses virus-triggered IFN-β induction via
300 interacting with MDA5 and MAVS to disrupt the formation of the MDA5–MAVS
301 complex (62). Furthermore, influenza A virus nonstructural protein 1 (NS1) interacts
302 with RIG-I and inhibits RIG-I ubiquitination to antagonize RIG-I-mediated IFN-β
303 production (51, 63). In this study, we found that PDCoV NS6 also interacts with
304 RIG-I/MDA5; however, differently from the mechanisms used by the viral proteins
305 mentioned above, PDCoV NS6 does not inhibit IFN-β production by overexpressing
306 RIG-I or MDA5. Moreover, NS6 also does not interact with MAVS and does not
307 disrupt the complex formation of RIG-I and MAVS, TBK1, or IKKε (data not shown),
308 which is not surprising given that NS6 does not inhibit the IFN-β promoter activity
309 induced by RIG-I, MDA5,MAVS, or their downstream molecules (Fig. 3).

310 Our results also demonstrate that PDCoV NS6 specifically interacts with the
311 CTD of RIG-I, however, it can interacts with the Hel and CTD of MDA5. RIG-I and
312 MDA5 have similar domain structures, possessing N-terminal tandem CARDs, a
313 central DExD/H-box type RNA helicase containing two RecA domains (Hel-1 and
314 Hel-2) with a family-specific insertion named Hel-2i within Hel-2, and a CTD (53, 64,
315 65). Based on the different molecular mechanisms for dsRNA recognition by MDA5
316 and RIG-I, especially the structural mechanism for the divergent RNA recognition by
317 RIG-I and MDA5 (65-68), the different interaction domain between RIG-I and MDA5

318 with NS6 is reasonable and can be explained. Previous studies demonstrated that the
319 RIG-I CTD caps the dsRNA end and plays a predominant role in high-affinity binding
320 and selectivity for dsRNA (66), while the MDA5 CTD binds to the dsRNA stem (65).
321 Differently from RIG-I helicase domain, MDA5 helicase domain also contributes to
322 the dsRNA stem recognition, and its role is beyond simply providing additional RNA
323 affinity but likely includes precise positioning of the CTD for efficient recognition of
324 the dsRNA stem (65). Interactions with the CTD of RIG-I and the Hel and CTD of
325 MDA5 make the NS6 to block the binding of RIG-I/MDA5 with dsRNA. Take RIG-I
326 for example, the binding of its CTD for viral RNA PAMPs can serve as the first step
327 in initiating the activation of downstream signaling pathways (64). In the ligand-free
328 state, the binding of CARDs to Hel-2i results in the formation of an auto-repressed
329 state for this protein by sterically hindering the access of ubiquitination enzymes and
330 of polyubiquitin binding to CARDs. Upon viral infection, the initial binding of viral
331 dsRNA to the CTD results in its functional transformation from an auto-repressed
332 state into a signaling competent configuration and the release of CARDs,
333 subsequently leading to the 2CARD oligomerization, followed by its interaction with
334 MAVS as described in Fig. 8C. However, the interaction between NS6 and the CTD
335 of RIG-I or the Hel and CTD of MDA5 appears to block the dsRNA binding sites
336 (CTDs or Hel), resulting in RIG-I/MDA5 having a reduced dsRNA-binding ability
337 and less subsequent type I IFN production. Because NS6 is not a RNA-binding
338 protein, the possibility that NS6 inhibits SeV/poly(I:C)-induced IFN-β production by
339 competing with RIG-I/MDA5 for dsRNA binding can be excluded (Fig. 7). Thus, it is

possible that NS6 competes with dsRNA for binding to RIG-I/MDA5. The competition binding experiment results (Fig. 8) support this hypothesis, which is illustrated in Fig. 8C using RIG-I as a representative receptor. Indeed, previous work has also shown that the overexpression of the CTD inhibits RIG-I-dependent signaling in response to SeV infection (69), and the possible mechanism for it is mediated through the sequestration of viral RNA produced during SeV infection (52). Overall, our experiments reveal that NS6 utilizes a mechanism that is different from those of other viral proteins previously reported to antagonize RLR-mediated IFN-β production.

The NS6 protein is unique to PDCoV with no significant homology to other viral proteins of known coronaviruses. Previous work has shown that PDCoV NS6 is expressed during early virus infection and is distributed in the cytoplasm (19). It seems likely that the early expression of NS6 proteins in virus-infected cells is important because their direct interaction with RIG-I or MDA5 functions to prevent the recognition viral dsRNA by these proteins. It should be noted that the identified function of NS6 to antagonize IFN production in the present study is derived from overexpression and should be further tested in the context of live virus infection. Regrettably, a PDCoV reverse genetics system was not available when this work was conducted, preventing further investigation of the NS6 IFN antagonist activity at the level of virus infection *in vivo*. We are currently working to establish a PDCoV reverse genetics system, which will allow the generation of mutant or deletion viruses that can be used to further explore the functions of NS6 protein, such as the effects of

362 NS6 deletion on the IFN-β production, viral replication, and/or host spectrum.

363 Interestingly, this study found that PDCoV NS6 appears to interact preferentially
364 with RNA-binding proteins, even though it is not a RNA-binding protein itself. In
365 addition to the well-known RNA-binding proteins RIG-I and MDA5, PDCoV N
366 protein was also found to be a RNA-binding protein (Fig. 7), and NS6 interacts with
367 N protein (data not shown). Our previous study showed that PDCoV NS6 is
368 associated with the purified viral particle, and NS6 is mainly localized in the
369 endoplasmic reticulum (ER) and ER-Golgi intermediate compartments, which are the
370 sites of coronavirus assembly and packaging (19). Whether or not the interaction
371 between NS6 and N protein is associated with viral replication and assembly is
372 currently under investigation in our laboratory, and the resulting findings will greatly
373 improve our understanding of the role of NS6 protein in viral replication and
374 pathogenicity.

375 In summary, we report that overexpression of accessory protein NS6 antagonizes
376 IFN-β production via interacting with RIG-I/MDA5 to impede their association with
377 dsRNA, leading to the blockage of the beginning PRRs-dsRNA-recognition step. To
378 date, only PDCoV nsp5 (70, 71) and NS6 protein (this study) have been identified as
379 IFN antagonists, while at least eight proteins encoded by SARS-CoV have been
380 identified as IFN antagonists (26, 27, 39, 72-74). The further identification and
381 characterization of PDCoV-encoded IFN antagonists will accelerate the elucidation of
382 the association between PDCoV and the IFN signaling pathway, which may lead to
383 the development of novel effective therapeutic strategies and vaccines.

384

385 **MATERIALS AND METHODS**

386 **Viruses and cells.** The PDCoV strain CHN-HN-2014 (GenBank accession number
387 KT336560) used in this study was isolated in China in 2014 from a piglet with severe
388 diarrhea (75). SeV was obtained from the Centre of Virus Resource and Information,
389 Wuhan Institute of Virology, Chinese Academy of Sciences. VSV-GFP was gifted by
390 Dr. Zhigao Bu at the Harbin Veterinary Research Institute of the Chinese Academy of
391 Agricultural Sciences. HEK-293T cells were obtained from the China Center for Type
392 Culture Collection and maintained at 37 °C in 5% CO_2 in Dulbecco's Modified
393 Eagle's medium (Invitrogen, USA) supplemented with 10% heat-inactivated fetal
394 bovine serum (FBS). The LLC-PK1 cells used for PDCoV propagation were
395 purchased from the ATCC (ATCC number CL-101) and grown under the same
396 conditions described above.

397

398 **Plasmids and dual-luciferase reporter assay.** The NS6 gene from PDCoV strain
399 CHN-HN-2014 was amplified with the primers PDCoV-NS6-F and PDCoV-NS6-R
400 **(Table 1)** and cloned into pCAGGS-HA-N with an N-terminal HA tag or
401 pCAGGS-Flag-N with an N-terminal Flag tag, and named pCAGGS-HA-NS6 and
402 pCAGGS-Flag-NS6, respectively. The PDCoV N gene was also cloned into
403 pCAGGS-Flag-N with an N-terminal Flag tag using the primers PDCoV-N-F and
404 PDCoV-N-R **(Table 1)**, and the resulting plasmid was named pCAGGS-Flag-NP. The
405 luciferase reporter plasmids IFN-β-Luc, NF-κB-Luc, and IRF3-Luc have been

406 described previously (76). The expression plasmids for Flag-tagged RIG-I and its
407 constitutively activated mutant (RIG-IN), MDA5, MAVS, TBK1, and IRF3 and its
408 constitutively activated mutant (IRF3-5D) have also been described previously (77).
409 The GFP expression plasmid (pEGFP-C1) was purchased from TaKaRa (Japan).
410 Three characteristic functional domains of RIG-I or MDA5, including the 2CARD
411 (RIG-I aa 1 to 228; MDA5 aa 1 to 295), the helicase domain (RIG-I aa 229 to 803;
412 MDA5 aa 296 to 827), and the CTD (RIG-I aa 804 to 925; MDA5 aa 828 to 1025),
413 were cloned into the pCAGGS-Flag-N vector using the primers listed in **Table 1**, and
414 the resulting expression constructs were named as pCAGGS-Flag-2CARD(RIG-I),
415 pCAGGS-Flag-2CARD(MDA5), pCAGGS-Flag-Hel(RIG-I),
416 pCAGGS-Flag-Hel(MDA5), pCAGGS-Flag-CTD(RIG-I), and
417 pCAGGS-Flag-CTD(MDA5), respectively. All plasmids were verified by sequencing.
418 For luciferase reporter assays, HEK-293T or LLC-PK1 cells grown in 24-well plates
419 were transfected using Lipofectamine 2000 (Invitrogen) with a luciferase reporter
420 plasmid (IFN-β-Luc, NF-κB-Luc, or IRF3-Luc) and pRL-TK (Promega), together
421 with the indicated expression plasmid or an empty vector. At 24 h after transfection,
422 the cells were stimulated with SeV (10 hemagglutinating activity units/well) or
423 poly(I:C) (InvivoGen, USA) for 12 h. Subsequently, the firefly luciferase and *Renilla*
424 luciferase activities from lysed cells were evaluated through the Dual-Luciferase
425 reporter assay system according to the instructions from the manufacturer (Promega).
426 Representative data from three independently conducted experiments are expressed as
427 the relative firefly luciferase activities with normalization to the *Renilla* luciferase

activities.

RNA extraction and quantitative real-time RT-PCR. To confirm the effects of NS6 protein on SeV replication, HEK-293T cells in 24-well plates were transfected with increasing amounts of NS6 expression plasmids. After 24 h, the cells were mock-infected or infected with SeV for 12 h. Total RNA was extracted from the treated cells with TRIzol reagent (Invitrogen), followed by first-strand cDNA synthesis by using avian myeloblastosis virus (AMV) reverse transcriptase (TaKaRa, Japan) with the indicated primers (**Table 1**). Each quantitative real-time PCR (qPCR) experiment was performed at least three times and was conducted via the SYBR green PCR assay (Applied Biosystems) using the cDNA described above as template. The results are expressed as the relative gene expression level with normalization to the expression level of glyceraldehyde-3-phosphate dehydrogenase (GAPDH).

IFN bioassay. To measure the effect of NS6 on the amount of IFN production by HEK-293T cells following stimulation by SeV, IFN bioassays were performed as described previously (54).

Western blot analysis. HEK-293T cells grown in 60-mm dishes were transfected with the indicated plasmids for 24 h. The cells were mock-infected or infected with SeV for 8 h. The transfected cells were harvested with lysis buffer (4% SDS, 3% dithiothreitol [DTT], 0.065 mM Tris-HCl [pH 6.8], 30% glycerin) supplemented with

450 a protease inhibitor cocktail and a phosphatase inhibitor cocktail (Sigma). Equal
451 amounts of proteins were subjected to separation by 12% SDS-PAGE and then
452 transferred to a polyvinylidene difluoride membrane, followed by blocking with 5%
453 nonfat milk in PBST with 0.1% polysorbate-20 and subsequent treatment with the
454 indicated primary antibodies, rabbit anti-p-IRF3, anti-p65 (ABclonal), anti-p-p65, and
455 anti-IRF3 (Cell Signaling Technology), and mouse anti-Flag or -HA antibodies (MBL)
456 at 37 °C for 4 h. After washing three times with PBST, the membranes were incubated
457 with horseradish peroxidase (HRP)-conjugated secondary antibodies (Beyotime,
458 China) for 45 min at room temperature. After washing three times, the membrane was
459 visualized by enhanced chemiluminescence reagents (ELC; BIO-RAD). The
460 expression levels of β-actin were detected with a mouse anti-β-actin monoclonal
461 antibody (MBL) and used as indicative of whether or not the protein sample loading
462 was equal.
463
464 **Co-IP and western blot analyses.** Co-IP assays were performed as described
465 previously (77). HEK-293T cells that had been cultured in 60-mm dishes were
466 co-transfected with the indicated expression plasmids containing Flag or HA tags.
467 After 28 h, the cells were harvested and lysed on ice with 0.5 ml of lysis buffer (50
468 mM Tris-HCl (pH 7.4), 150 mM NaCl, 1% NP-40, 10% glycerin, 0.1% SDS, and 2
469 mM Na_2EDTA) for 30 min at 4 °C. A portion of each supernatant from the lysed cells
470 was used in the whole-cell extract assays. The remaining portions of the supernatants
471 from the lysed cells were immunoprecipitated with affinity antibodies overnight at

4 °C and then treated with protein A+G agarose beads (Beyotime) for 5 h at 4 °C. The beads containing immunoprecipitates were washed three times with 1 ml of lysis buffer. Whole-cell extracts and immunoprecipitates were resuspended in SDS-PAGE loading buffer, boiled at 95 °C for 5 min, and then subjected to 12% SDS-PAGE and transferred to polyvinylidene difluoride membrane, followed by western blot analyses with the indicated antibodies.

Poly(I:C) pulldown assay. HEK-293T cells grown in 60-mm plates were transfected with 4 μg of each of the indicated expression plasmids, including Flag-tagged RIG-I, N and NS6, or empty vector for 24 h. The cells were harvested and lysed on ice with 400 μl of lysis buffer (50 mM Tris-HCl (pH 7.4), 150 mM NaCl, 1% NP-40, 10% glycerin, 0.1% SDS, and 2 mM Na_2EDTA) supplemented with a cocktail of protease inhibitors (Sigma). The clarified cell lysates were mixed with a prepared suspension of poly(I:C)-coated agarose beads and incubated for 4 h at 4 °C. The beads were washed three times with 1 ml of lysis buffer by multiple centrifugations and then subjected to western blotting analysis by using mouse anti-Flag antibody (MBL) as the primary antibody, followed by treatment with HRP-conjugated goat anti-mouse IgG.

Indirect immunofluorescence assay (IFA). Monolayers of HEK-293T cells seeded onto coverslips in 24-well plates were transfected with pCAGGS-HA-NS6 or empty vector for 24 h. The cells were then mock-infected or infected with SeV for 8 h. The

494 cells were subsequently fixed with 4% paraformaldehyde for 15 min and then
495 permeated with methyl alcohol for 10 min at room temperature. After three washes
496 with PBST, the cells were blocked with PBST containing 5% bovine serum albumin
497 (BSA) for 1 h, followed by incubation separately with a rabbit polyclonal antibody
498 against IRF3 (1:200) or against p65 (1:200) or a mouse anti-HA antibody (1:200) for
499 1 h at 37 °C. The cells were then stained with secondary antibodies Alexa Fluor
500 594-conjugated donkey anti-mouse IgG and Alexa Fluor 488-conjugated donkey
501 anti-rabbit IgG (Santa Cruz Biotechnology) for 1 h at 37 °C, followed by treatment
502 with 4′, 6-diamidino-2-phenylindole (DAPI) (Beyotime) for 15 min at room
503 temperature. Fluorescent images were visualized with the use of a confocal laser
504 scanning microscope (Fluoviewver.3.1; Olympus, Japan).
505
506 **Statistical analysis.** Statistical differences were determined by one-way ANOVAs
507 using GraphPad Prism 5.0 software. For all experiments, differences were considered
508 to be statistically significant when p values were <0.05.
509
510 **ACKNOWLEDGEMENTS**
511 We thank Dr. Zhigao Bu for providing VSV-GFP recombinant virus. This work was
512 supported by the National Natural Science Foundation of China (31730095), the
513 National Key R&D Plan of China (2016YFD0500103), the Key Technology R&D
514 Programme of China (2015BAD12B02), and the Major S&T Project of Hubei
515 Province (2017ABA138).

516

517 **REFERENCES**

518 1. **Jung K, Hu H, Eyerly B, Lu Z, Chepngeno J, Saif LJ.** 2015. Pathogenicity of 2 porcine
519 deltacoronavirus strains in gnotobiotic pigs. Emerg Infect Dis **21:**650-654.

520 2. **Hu H, Jung K, Vlasova AN, Saif LJ.** 2016. Experimental infection of gnotobiotic pigs
521 with the cell-culture-adapted porcine deltacoronavirus strain OH-FD22. Arch Virol
522 **161:**3421-3434.

523 3. **Ma Y, Zhang Y, Liang X, Lou F, Oglesbee M, Krakowka S, Li J.** 2015. Origin, evolution,
524 and virulence of porcine deltacoronaviruses in the United States. MBio **6:**e00064.

525 4. **Woo PC, Lau SK, Lam CS, Lau CC, Tsang AK, Lau JH, Bai R, Teng JL, Tsang CC,**
526 **Wang M, Zheng BJ, Chan KH, Yuen KY.** 2012. Discovery of seven novel Mammalian
527 and avian coronaviruses in the genus deltacoronavirus supports bat coronaviruses as
528 the gene source of alphacoronavirus and betacoronavirus and avian coronaviruses as
529 the gene source of gammacoronavirus and deltacoronavirus. J Virol **86:**3995-4008.

530 5. **Marthaler D, Jiang Y, Collins J, Rossow K.** 2014. Complete Genome Sequence of
531 Strain SDCV/USA/Illinois121/2014, a Porcine Deltacoronavirus from the United States.
532 Genome Announc **2:** e00218-14.

533 6. **Marthaler D, Raymond L, Jiang Y, Collins J, Rossow K, Rovira A.** 2014. Rapid
534 detection, complete genome sequencing, and phylogenetic analysis of porcine
535 deltacoronavirus. Emerg Infect Dis **20:**1347-1350.

536 7. **Wang L, Byrum B, Zhang Y.** 2014. Detection and genetic characterization of
537 deltacoronavirus in pigs, Ohio, USA, 2014. Emerg Infect Dis **20:**1227-1230.

538 8. **Wang L, Byrum B, Zhang Y.** 2014. Porcine coronavirus HKU15 detected in 9 US
539 states, 2014. Emerg Infect Dis **20:**1594-1595.
540 9. **Li G, Chen Q, Harmon KM, Yoon KJ, Schwartz KJ, Hoogland MJ, Gauger PC, Main**
541 **RG, Zhang J.** 2014. Full-Length Genome Sequence of Porcine Deltacoronavirus
542 Strain USA/IA/2014/8734. Genome Announc **2:** e00278-14.
543 10. **Lee S, Lee C.** 2014. Complete Genome Characterization of Korean Porcine
544 Deltacoronavirus Strain KOR/KNU14-04/2014. Genome Announc **2:** e01191-14.
545 11. **Dong N, Fang L, Zeng S, Sun Q, Chen H, Xiao S.** 2015. Porcine Deltacoronavirus in
546 Mainland China. Emerg Infect Dis **21:**2254-2255.
547 12. **Wang YW, Yue H, Fang W, Huang YW.** 2015. Complete Genome Sequence of
548 Porcine Deltacoronavirus Strain CH/Sichuan/S27/2012 from Mainland China.
549 Genome Announc **3:** e00945-15.
550 13. **Song D, Zhou X, Peng Q, Chen Y, Zhang F, Huang T, Zhang T, Li A, Huang D, Wu Q,**
551 **He H, Tang Y.** 2015. Newly Emerged Porcine Deltacoronavirus Associated With
552 Diarrhoea in Swine in China: Identification, Prevalence and Full-Length Genome
553 Sequence Analysis. Transbound Emerg Dis **62:**575-580.
554 14. **Janetanakit T, Lumyai M, Bunpapong N, Boonyapisitsopa S, Chaiyawong S,**
555 **Nonthabenjawan N, Kesdaengsakonwut S, Amonsin A.** 2016. Porcine
556 Deltacoronavirus, Thailand, 2015. Emerg Infect Dis **22:**757-759.
557 15. **Lorsirigool A, Saeng-Chuto K, Temeeyasen G, Madapong A, Tripipat T, Wegner M,**
558 **Tuntituvanont A, Intrakamhaeng M, Nilubol D.** 2016. The first detection and full-length
559 genome sequence of porcine deltacoronavirus isolated in Lao PDR. Arch Virol

161:2909-2911.

16. **Saeng-Chuto K, Lorsirigool A, Temeeyasen G, Vui DT, Stott CJ, Madapong A, Tripipat T, Wegner M, Intrakamhaeng M, Chongcharoen W, Tantituvanont A, Kaewprommal P, Piriyapongsa J, Nilubol D.** 2017. Different Lineage of Porcine Deltacoronavirus in Thailand, Vietnam and Lao PDR in 2015. Transbound Emerg Dis **64:**3-10.

17. **Zhang J.** 2016. Porcine deltacoronavirus: Overview of infection dynamics, diagnostic methods, prevalence and genetic evolution. Virus Res **226:**71-84.

18. **Jung K, Hu H, Saif LJ.** 2017. Calves are susceptible to infection with the newly emerged porcine deltacoronavirus, but not with the swine enteric alphacoronavirus, porcine epidemic diarrhea virus. Arch Virol **162:** 2357-2362.

19. **Fang P, Fang L, Liu X, Hong Y, Wang Y, Dong N, Ma P, Bi J, Wang D, Xiao S.** 2016. Identification and subcellular localization of porcine deltacoronavirus accessory protein NS6. Virology **499:**170-177.

20. **Fang P, Fang L, Hong Y, Liu X, Dong N, Ma P, Bi J, Wang D, Xiao S.** 2017. Discovery of a novel accessory protein NS7a encoded by porcine deltacoronavirus. J Gen Virol **98:**173-178.

21. **Lee S, Lee C.** 2015. Functional characterization and proteomic analysis of the nucleocapsid protein of porcine deltacoronavirus. Virus Res **208:**136-145.

22. **Liu DX, Fung TS, Chong KK, Shukla A, Hilgenfeld R.** 2014. Accessory proteins of SARS-CoV and other coronaviruses. Antiviral Res **109:**97-109.

23. **Yount B, Roberts RS, Sims AC, Deming D, Frieman MB, Sparks J, Denison MR, Davis N, Baric RS.** 2005. Severe acute respiratory syndrome coronavirus

group-specific open reading frames encode nonessential functions for replication in cell cultures and mice. J Virol **79:**14909-14922.

24. **Tan YJ, Lim SG, Hong W.** 2006. Understanding the accessory viral proteins unique to the severe acute respiratory syndrome (SARS) coronavirus. Antiviral Res **72:**78-88.

25. **Fischer F, Peng D, Hingley ST, Weiss SR, Masters PS.** 1997. The internal open reading frame within the nucleocapsid gene of mouse hepatitis virus encodes a structural protein that is not essential for viral replication. J Virol **71:**996-1003.

26. **Kopecky-Bromberg SA, Martinez-Sobrido L, Frieman M, Baric RA, Palese P.** 2007. Severe acute respiratory syndrome coronavirus open reading frame (ORF) 3b, ORF 6, and nucleocapsid proteins function as interferon antagonists. J Virol **81:**548-557.

27. **Shi CS, Qi HY, Boularan C, Huang NN, Abu-Asab M, Shelhamer JH, Kehrl JH.** 2014. SARS-coronavirus open reading frame-9b suppresses innate immunity by targeting mitochondria and the MAVS/TRAF3/TRAF6 signalosome. J Immunol **193:**3080-3089.

28. **Zhou H, Ferraro D, Zhao J, Hussain S, Shao J, Trujillo J, Netland J, Gallagher T, Perlman S.** 2010. The N-terminal region of severe acute respiratory syndrome coronavirus protein 6 induces membrane rearrangement and enhances virus replication. J Virol **84:**3542-3551.

29. **Niemeyer D, Zillinger T, Muth D, Zielecki F, Horvath G, Suliman T, Barchet W, Weber F, Drosten C, Muller MA.** 2013. Middle East respiratory syndrome coronavirus accessory protein 4a is a type I interferon antagonist. J Virol **87:**12489-12495.

30. **Thornbrough JM, Jha BK, Yount B, Goldstein SA, Li YZ, Elliott R, Sims AC, Baric RS, Silverman RH, Weiss SR.** 2016. Middle East Respiratory Syndrome Coronavirus

604 NS4b Protein Inhibits Host RNase L Activation. MBio **7:** e00258.

605 31. **Matthews KL, Coleman CM, van der Meer Y, Snijder EJ, Frieman MB.** 2014. The
606 ORF4b-encoded accessory proteins of Middle East respiratory syndrome coronavirus
607 and two related bat coronaviruses localize to the nucleus and inhibit innate immune
608 signalling. J Gen Virol **95:**874-882.

609 32. **Zhao L, Jha BK, Wu A, Elliott R, Ziebuhr J, Gorbalenya AE, Silverman RH, Weiss SR.**
610 2012. Antagonism of the interferon-induced OAS-RNase L pathway by murine
611 coronavirus ns2 protein is required for virus replication and liver pathology. Cell Host
612 Microbe **11:**607-616.

613 33. **Zhang R, Jha BK, Ogden KM, Dong B, Zhao L, Elliott R, Patton JT, Silverman RH,**
614 **Weiss SR.** 2013. Homologous 2',5'-phosphodiesterases from disparate RNA viruses
615 antagonize antiviral innate immunity. Proc Natl Acad Sci U S A **110:**13114-13119.

616 34. **Kato H, Takahasi K, Fujita T.** 2011. RIG-I-like receptors: cytoplasmic sensors for
617 non-self RNA. Immunol Rev **243:**91-98.

618 35. **Deng X, Hackbart M, Mettelman RC, O'Brien A, Mielech AM, Yi G, Kao CC, Baker SC.**
619 2017. Coronavirus nonstructural protein 15 mediates evasion of dsRNA sensors and
620 limits apoptosis in macrophages. Proc Natl Acad Sci U S A **114:**E4251-E4260.

621 36. **Zhou H, Perlman S.** 2007. Mouse hepatitis virus does not induce Beta interferon
622 synthesis and does not inhibit its induction by double-stranded RNA. J Virol
623 **81:**568-574.

624 37. **Meylan E, Curran J, Hofmann K, Moradpour D, Binder M, Bartenschlager R, Tschopp**
625 **R.** 2005. Cardif is an adaptor protein in the RIG-I antiviral pathway and is targeted by

hepatitis C virus. Nature **437:**1167-1172.

38. **Seth RB, Sun L, Ea CK, Chen ZJ.** 2005. Identification and characterization of MAVS, a mitochondrial antiviral signaling protein that activates NF-kappaB and IRF 3. Cell **122:**669-682.

39. **Siu KL, Kok KH, Ng MH, Poon VK, Yuen KY, Zheng BJ, Jin DY.** 2009. Severe acute respiratory syndrome coronavirus M protein inhibits type I interferon production by impeding the formation of TRAF3.TANK.TBK1/IKKepsilon complex. J Biol Chem **284:**16202-16209.

40. **Zhang Q, Shi K, Yoo D.** 2016. Suppression of type I interferon production by porcine epidemic diarrhea virus and degradation of CREB-binding protein by nsp1. Virology **489:**252-268.

41. **Totura AL, Baric RS.** 2012. SARS coronavirus pathogenesis: host innate immune responses and viral antagonism of interferon. Curr Opin Virol **2:**264-275.

42. **Clementz MA, Chen Z, Banach BS, Wang Y, Sun L, Ratia K, Baez-Santos YM, Wang J, Takayama J, Ghosh AK, Li K, Mesecar AD, Baker SC.** 2010. Deubiquitinating and interferon antagonism activities of coronavirus papain-like proteases. J Virol **84:**4619-4629.

43. **Roth-Cross JK, Martinez-Sobrido L, Scott EP, Garcia-Sastre A, Weiss SR.** 2007. Inhibition of the alpha/beta interferon response by mouse hepatitis virus at multiple levels. J Virol **81:**7189-7199.

44. **Channappanavar R, Fehr AR, Vijay R, Mack M, Zhao J, Meyerholz DK, Perlman S.** 2016. Dysregulated Type I Interferon and Inflammatory Monocyte-Macrophage

Responses Cause Lethal Pneumonia in SARS-CoV-Infected Mice. Cell Host Microbe **19:**181-193.

45. **Luo J, Fang L, Dong N, Fang P, Ding Z, Wang D, Chen H, Xiao S.** 2016. Porcine deltacoronavirus (PDCoV) infection suppresses RIG-I-mediated interferon-beta production. Virology **495:**10-17.

46. **Xu K, Zheng BJ, Zeng R, Lu W, Lin YP, Xue L, Li L, Yang LL, Xu C, Dai J, Wang F, Li Q, Dong QX, Yang RF, Wu JR, Sun B.** 2009. Severe acute respiratory syndrome coronavirus accessory protein 9b is a virion-associated protein. Virology **388:**279-285.

47. **Huang C, Peters CJ, Makino S.** 2007. Severe acute respiratory syndrome coronavirus accessory protein 6 is a virion-associated protein and is released from 6 protein-expressing cells. J Virol **81:**5423-5426.

48. **Frieman M, Yount B, Heise M, Kopecky-Bromberg SA, Palese P, Baric RS.** 2007. Severe acute respiratory syndrome coronavirus ORF6 antagonizes STAT1 function by sequestering nuclear import factors on the rough endoplasmic reticulum/Golgi membrane. J Virol **81:**9812-9824.

49. **Sato M, Tanaka N, Hata N, Oda E, Taniguchi T.** 1998. Involvement of the IRF family transcription factor IRF-3 in virus-induced activation of the IFN-beta gene. FEBS Lett **425:**112-116.

50. **Wathelet MG, Lin CH, Parekh BS, Ronco LV, Howley PM, Maniatis T.** 1998. Virus infection induces the assembly of coordinately activated transcription factors on the IFN-beta enhancer in vivo. Mol Cell **1:**507-518.

51. **Mibayashi M, Martinez-Sobrido L, Loo YM, Cardenas WB, Gale M, Jr., Garcia-Sastre**

670 **A.** 2007. Inhibition of retinoic acid-inducible gene I-mediated induction of beta
671 interferon by the NS1 protein of influenza A virus. J Virol **81:**514-524.
672 52. **Yoneyama M, Kikuchi M, Natsukawa T, Shinobu N, Imaizumi T, Miyagishi M, Taira K,**
673 **Akira S, Fujita T.** 2004. The RNA helicase RIG-I has an essential function in
674 double-stranded RNA-induced innate antiviral responses. Nat Immunol **5:**730-737.
675 53. **Luo D, Ding SC, Vela A, Kohlway A, Lindenbach BD, Pyle AM.** 2011. Structural
676 insights into RNA recognition by RIG-I. Cell **147:**409-422.
677 54. **Cardenas WB, Loo YM, Gale M, Jr., Hartman AL, Kimberlin CR, Martinez-Sobrido L,**
678 **Saphire EO, Basler CF.** 2006. Ebola virus VP35 protein binds double-stranded RNA
679 and inhibits alpha/beta interferon production induced by RIG-I signaling. J Virol
680 **80:**5168-5178.
681 55. **Chang CK, Hsu YL, Chang YH, Chao FA, Wu MC, Huang YS, Hu CK, Huang TH.**
682 2009. Multiple nucleic acid binding sites and intrinsic disorder of severe acute
683 respiratory syndrome coronavirus nucleocapsid protein: implications for
684 ribonucleocapsid protein packaging. J Virol **83:**2255-2264.
685 56. **Zeng LP, Gao YT, Ge XY, Zhang Q, Peng C, Yang XL, Tan B, Chen J, Chmura AA,**
686 **Daszak P, Shi ZL.** 2016. Bat Severe Acute Respiratory Syndrome-Like Coronavirus
687 WIV1 Encodes an Extra Accessory Protein, ORFX, Involved in Modulation of the Host
688 Immune Response. J Virol **90:**6573-6582.
689 57. **Zou J, Chang M, Nie P, Secombes CJ.** 2009. Origin and evolution of the RIG-I like
690 RNA helicase gene family. BMC Evol Biol **9:**85.
691 58. **Roth-Cross JK, Bender SJ, Weiss SR.** 2008. Murine coronavirus mouse hepatitis virus

is recognized by MDA5 and induces type I interferon in brain macrophages/microglia. J Virol **82:**9829-9838.

59. **Zalinger ZB, Elliott R, Rose KM, Weiss SR.** 2015. MDA5 Is Critical to Host Defense during Infection with Murine Coronavirus. J Virol **89:**12330-12340.

60. **Fan L, Briese T, Lipkin WI.** 2010. Z proteins of New World arenaviruses bind RIG-I and interfere with type I interferon induction. J Virol **84:**1785-1791.

61. **Ling Z, Tran KC, Teng MN.** 2009. Human respiratory syncytial virus nonstructural protein NS2 antagonizes the activation of beta interferon transcription by interacting with RIG-I. J Virol **83:**3734-3742.

62. **Wang XM, Li Y, Mao AP, Li C, Li YK, Tien P.** 2010. Hepatitis B virus X protein suppresses virus-triggered IRF3 activation and IFN-beta induction by disrupting the VISA-associated complex. Cellular & Molecular Immunology **7:**341-348.

63. **Gack MU, Albrecht RA, Urano T, Inn KS, Huang IC, Carnero E, Farzan M, Inoue S, Jung JU, Garcia-Sastre A.** 2009. Influenza A virus NS1 targets the ubiquitin ligase TRIM25 to evade recognition by the host viral RNA sensor RIG-I. Cell Host Microbe **5:**439-449.

64. **Kolakofsky D, Kowalinski E, Cusack S.** 2012. A structure-based model of RIG-I activation. RNA **18:**2118-2127.

65. **Wu B, Peisley A, Richards C, Yao H, Zeng X, Lin C, Chu F, Walz T, Hur S.** 2013. Structural basis for dsRNA recognition, filament formation, and antiviral signal activation by MDA5. Cell **152:**276-289.

66. **Cui S, Eisenacher K, Kirchhofer A, Brzozka K, Lammens A, Lammens K, Fujita T,**

714 **Conzelmann KK, Krug A, Hopfner KP.** 2008. The C-terminal regulatory domain is the
715 RNA 5'-triphosphate sensor of RIG-I. Mol Cell **29:**169-179.
716 67. **Li X, Lu C, Stewart M, Xu H, Strong RK, Igumenova T, Li P.** 2009. Structural basis of
717 double-stranded RNA recognition by the RIG-I like receptor MDA5. Arch Biochem
718 Biophys **488:**23-33.
719 68. **Wang Y, Ludwig J, Schuberth C, Goldeck M, Schlee M, Li H, Juranek S, Sheng G,**
720 **Micura R, Tuschl T, Hartmann G, Patel DJ.** 2010. Structural and functional insights
721 into 5'-ppp RNA pattern recognition by the innate immune receptor RIG-I. Nat Struct
722 Mol Biol **17:**781-787.
723 69. **Saito T, Hirai R, Loo YM, Owen D, Johnson CL, Sinha SC, Akira S, Fujita T, Gale M.**
724 2007. Regulation of innate antiviral defenses through a shared repressor domain in
725 RIG-I and LGP2. Proc Natl Acad Sci U S A **104:**582-587.
726 70. **Zhu X, Fang L, Wang D, Yang Y, Chen J, Ye X, Foda MF, Xiao S.** 2017. Porcine
727 deltacoronavirus nsp5 inhibits interferon-beta production through the cleavage of
728 NEMO. Virology **502:**33-38.
729 71. **Zhu X, Wang D, Zhou J, Pan T, Chen J, Yang Y, Lv M, Ye X, Peng G, Fang L, Xiao S.**
730 2017. Porcine Deltacoronavirus nsp5 Antagonizes Type I Interferon Signaling by
731 Cleaving STAT2. J Virol **91:** e00003-17.
732 72. **Li SW, Wang CY, Jou YJ, Huang SH, Hsiao LH, Wan L, Lin YJ, Kung SH, Lin CW.**
733 2016. SARS Coronavirus Papain-Like Protease Inhibits the TLR7 Signaling Pathway
734 through Removing Lys63-Linked Polyubiquitination of TRAF3 and TRAF6. Int J Mol
735 Sci **17:** E678.

736 73. **Jauregui AR, Savalia D, Lowry VK, Farrell CM, Wathelet MG.** 2013. Identification of
737 residues of SARS-CoV nsp1 that differentially affect inhibition of gene expression and
738 antiviral signaling. PLoS One **8:**e62416.
739 74. **Frieman M, Ratia K, Johnston RE, Mesecar AD, Baric RS.** 2009. Severe acute
740 respiratory syndrome coronavirus papain-like protease ubiquitin-like domain and
741 catalytic domain regulate antagonism of IRF3 and NF-kappaB signaling. J Virol
742 **83:**6689-6705.
743 75. **Dong N, Fang L, Yang H, Liu H, Du T, Fang P, Wang D, Chen H, Xiao S.** 2016.
744 Isolation, genomic characterization, and pathogenicity of a Chinese porcine
745 deltacoronavirus strain CHN-HN-2014. Vet Microbiol **196:**98-106.
746 76. **Wang D, Fang L, Shi Y, Zhang H, Gao L, Peng G, Chen H, Li K, Xiao S.** 2015. Porcine
747 Epidemic Diarrhea Virus 3C-Like Protease Regulates Its Interferon Antagonism by
748 Cleaving NEMO. J Virol **90:**2090-2101.
749 77. **Ding Z, Fang L, Jing H, Zeng S, Wang D, Liu L, Zhang H, Luo R, Chen H, Xiao S.**
750 2014. Porcine epidemic diarrhea virus nucleocapsid protein antagonizes beta
751 interferon production by sequestering the interaction between IRF3 and TBK1. J Virol
752 **88:**8936-8945.

753 **FIGURE LEGENDS**

754 **Fig. 1. NS6 inhibits SeV-mediated IFN-β production.** (**A and B**) HEK-293T cells
755 (A) or LLC-PK1 cells (B) cultured in 24-well plates were transfected with IFN-β-Luc
756 plasmid and pRL-TK plasmid, together with increasing amounts (0.2, 0.4, or 0.8 μg)
757 of plasmid pCAGGS-HA-NS6. At 24 h after transfection, cells were left untreated or
758 were infected with SeV (10 hemagglutination units/well). The cells were then
759 subjected to dual-luciferase assays at 12 h post-infection. The expression of PDCoV
760 NS6 protein was confirmed by western blot with an anti-HA antibody. β-actin served
761 as a protein loading control. (**C**) HEK-293T cells were transfected with the indicated
762 amounts of pCAGGS-HA-NS6 or empty vector. At 24 h after transfection, the cells
763 were infected with SeV for 12 h, after which cell supernatants were harvested.
764 Following UV irradiation, the harvested cell supernatants were overlaid onto fresh
765 HEK-293T cells in 24-well plates. At 24 h after treatment, the cells were infected with
766 VSV-GFP, and 12 h post-infection, virus replication was detected via fluorescence
767 microscopy. (**D**) HEK-293T cells grown in 24-well plates were transfected with
768 increasing quantities of pCAGGS-HA-NS6 or corresponding amounts of empty vector.
769 At 24 h after transfection, cells were infected with SeV for 12 h. The total RNA was
770 then extracted, and the SeV HN gene expression level was analyzed via quantitative
771 real-time RT-PCR, with normalization to the GAPDH gene expression level. The
772 results shown are representative of data from three independent experiments, $**p <$
773 0.01; $***p < 0.001$. Non-significant differences in data are indicated as "ns".
774

775 **Fig. 2. NS6 inhibits activation of IRF3 and NF-κB.** (**A and B**) HEK-293T cells
776 were transfected with the indicated amounts of pCAGGS-HA-NS6 or empty vector,
777 together with IRF3-Luc (A) or NF-κB-Luc (B) and pRL-TK plasmids, followed by
778 stimulation with SeV, and they were analyzed as described in Fig. 1A. Anti-HA
779 antibody was used to detect the expression of PDCoV NS6, and anti-β-actin antibody
780 was used to detect β-actin protein by western blot, which served as a protein loading
781 control. (**C and D**) HEK-293T cells were transfected with pCAGGS-HA-NS6 or
782 empty vector. After 24 h, the cells were infected with SeV or left untreated for 8 h.
783 Cell lysates were collected for western blot analysis with primary antibodies against
784 phosphorylated IRF3 (p-IRF3 Ser386) and total IRF3 (C) or phosphorylated p65
785 (p-p65 Ser536) and total p65 (D), HA, and β-actin. (**E and F**) HEK-293T cells were
786 transfected with pCAGGS-HA-NS6 or empty vector, followed by mock infection or
787 SeV infection for 8h as described for panels C and D. The cells were then fixed and
788 subjected to an immunofluorescence assay with rabbit anti-IRF3 and anti-p65 and
789 mouse anti-HA antibodies as primary antibodies, followed by staining with secondary
790 antibodies Alexa Fluor 488-conjugated donkey anti-rabbit IgG (green) or Alexa Fluor
791 594-conjugated donkey anti-mouse IgG (red). DAPI staining (blue) indicates the
792 locations of the cell nuclei. Fluorescent images were acquired with a confocal laser
793 scanning microscope (Fluoview ver. 3.1; Olympus, Japan). *$p < 0.05$; **$p < 0.01$;
794 ***$p < 0.001$.
795
796 **Fig. 3. NS6 fails to inhibit IFN-β production induced by RLR signaling pathway**

797 **molecules.** HEK-293T cells were transfected with IFN-β–Luc, pRL-TK, and
798 pCAGGS-HA-NS6 along with constructs expressing RIG-I/RIG-IN (A), MDA5 (B),
799 MAVS (C), TBK1, IKKε (D), or IRF3 (E). Dual-luciferase assays were performed 28
800 h after transfection. The relative firefly luciferase activity was relative to that of an
801 untreated empty vector control, with normalization to the *Renilla reniformis* luciferase
802 activity. The presented results represent the means and standard deviations of data
803 from three independent experiments. The expression of NS6 protein was verified by
804 western blot with anti-HA antibody. β-actin served as a protein loading control.
805
806 **Fig. 4. NS6 disrupts the IFN-β promoter activation induced by RIG-I or MDA5**
807 **coupled with SeV or poly(I:C).** HEK-293T cells were transfected with IFN-β–Luc,
808 pRL-TK, and the other indicated expression plasmids. At 24 h after transfection, cells
809 were stimulated with SeV/poly(I:C) or were left untreated for 12 h. Dual-luciferase
810 assays were then performed as described in Fig. 3. The presented results represent the
811 means and standard deviations of data from three independent experiments, ***$p <$
812 0.001. Western blot analysis with anti-HA antibody shows the expression of NS6
813 protein, and western blot for β-actin served as a protein loading control.
814
815 **Fig. 5. NS6 interacts with both RIG-I and MDA5.** (**A–D**) HEK-293T cells were
816 co-transfected with pCAGGS-HA-NS6 and Flag-tagged RIG-I (A and C), or
817 Flag-tagged MDA5 (B and D), respectively. At 28 h after transfection, cells were
818 lysed and subjected to immunoprecipitation analysis with anti-HA (IP: HA) or

819 anti-Flag (IP: Flag) antibody. The whole-cell lysates (WCL) and immunoprecipitation
820 (IP) complexes were analyzed via western blotting using anti-Flag, anti-HA, or
821 anti-β-actin antibodies. (**E and F**) HEK-293T cells were co-transfected with
822 pCAGGS-HA-NS6 and Flag-tagged RIG-I (E) or MDA5 (F). At 28 h after
823 transfection, the cells were fixed for immunofluorescence assays to detect NS6
824 protein (red) and RIG-I or MDA5 (green) with anti-HA and anti-Flag antibodies,
825 respectively. (**G and H**) HEK-293T cells were transfected with pCAGGS-HA-NS6
826 and pEGFP-C1, Flag-tagged RIG-I (G) or MDA5 (H) expression plasmids for 24 h,
827 followed by the transfection of poly(I:C). Cells were lysed 36 h after transfection, and
828 the clarified supernatants were left untreated or were treated with RNase A (50 μg/ml).
829 The samples were then subjected to immunoprecipitation assays using anti-HA MAb
830 (IP: HA). Cell lysates and immunoprecipitated complexes were subjected to western
831 blot assays as described in panels A and B.
832
833 **Fig. 6. NS6 interacts with the carboxyl terminus domain of RIG-I or the helicase**
834 **and carboxyl terminus domains of MDA5.** HEK293T cells were co-transfected
835 with pCAGGS-HA-NS6 and the expression plasmids encoding the 2CARD, Hel or
836 CTD of RIG-I/MDA5. Immunoprecipitation assays with anti-HA (A and B) or
837 anti-Flag (C and D) antibody (IP: HA or IP: Flag, respectively), and western blot
838 analysis were performed as described for Fig. 5A and 5C.
839
840 **Fig. 7. NS6 is not a RNA binding protein.** HEK-293T cells were transfected with

841 plasmids encoding Flag-tagged RIG-I protein, PDCoV NS6 and N protein, or empty
842 vector, respectively. Cells were lysed 28 h after transfection, and the resulting
843 supernatants were incubated with poly(C)- or poly(I:C)-coated agarose beads for 4 h
844 at 4 °C. The beads were then washed three times with lysis buffer by centrifugation,
845 followed by western blotting analysis with mouse anti-Flag antibody. The
846 poly(I:C)-coated agarose beads (pIC-beads) were prepared from poly(C)-coated beads
847 (pC-beads; Sigma) by incubating them with an equal volume of 2 mg of poly(I)
848 (Sigma) per ml for 1 h at 56 °C.
849
850 **Fig. 8. NS6 hinders the combination of dsRNA with RIG-I/MDA5.** (**A and B**)
851 HEK-293T cells were individually transfected with plasmids encoding Flag-tagged
852 RIG-I (A), MDA5 (B), and increasing quantities of NS6 expression plasmids for 28 h.
853 Lysates from the cells overexpressing NS6 were incubated with an equal volume of
854 lysates from cells overexpressing RIG-I or MDA5, followed by treatment with
855 poly(I:C)-coated agarose beads for 4 h at 4 °C. The beads were then washed three
856 times with lysis buffer by centrifugation and subjected to western blotting analysis as
857 described in Fig. 7. The number below pictures represents the relative level of
858 RIG-I/MDA5 compared to control group via Image J software analysis. (**C**) A
859 schematic diagram, using RIG-I acts as a representative protein, of the mechanism for
860 NS6 protein inhibition of the RLR signaling pathway. In the inactivated state of RIG-I,
861 the CARDs are bound to Hel-2i, which is unavailable for downstream signaling in this
862 auto-inhibited state. The CTD, which is tethered to the red bridging helix by a flexible

linker, is able to sense RNA PAMPs. Upon virus infection, the CTD-bound dsRNA is pre-oriented to form a network of interactions with the helicase domains Hel-1 and Hel-2i, but not Hel-2, leading to the segregation of interaction of CARDs with Hel-2i and the subsequent availability for interaction with downstream signaling molecules (64).

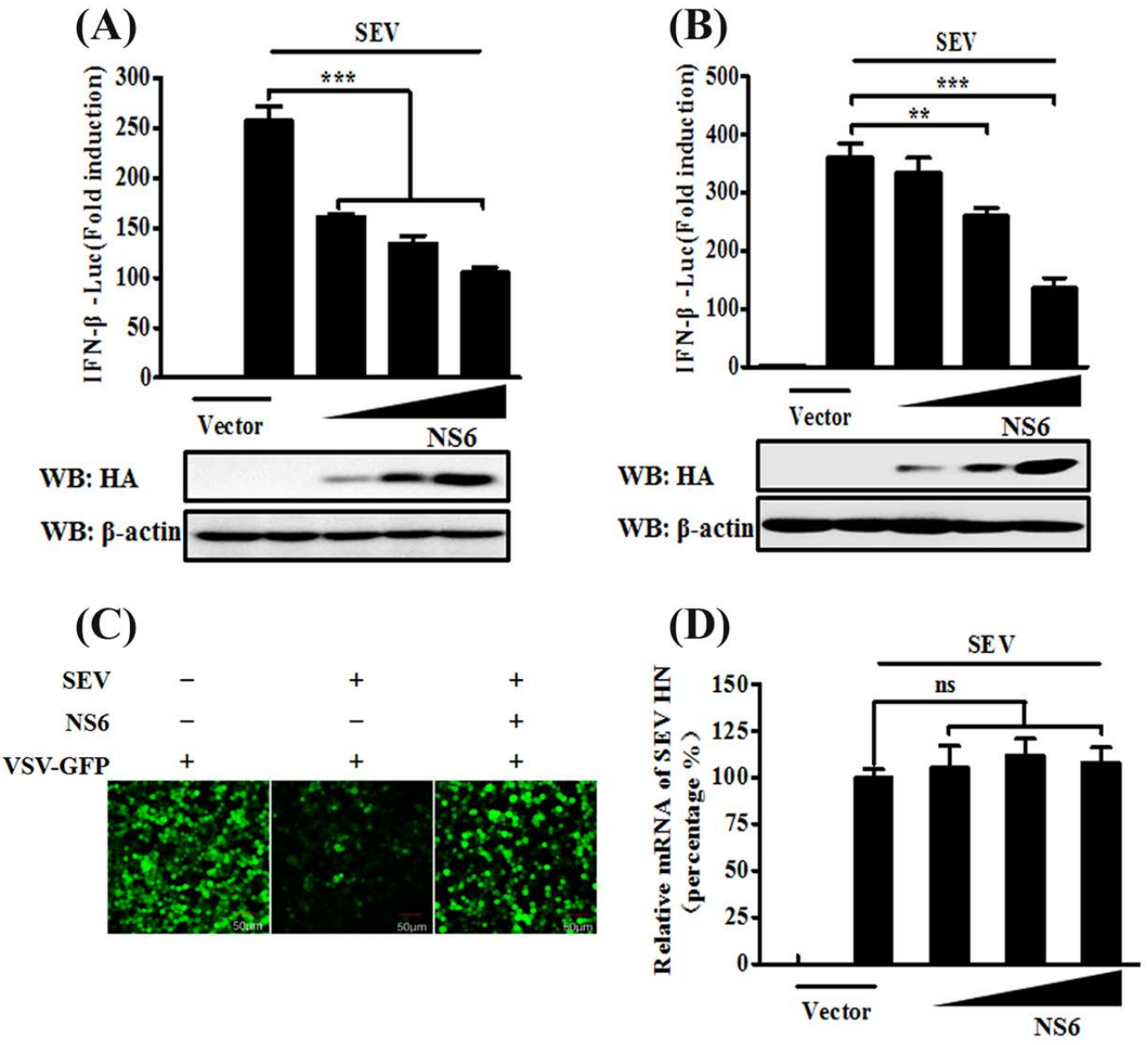

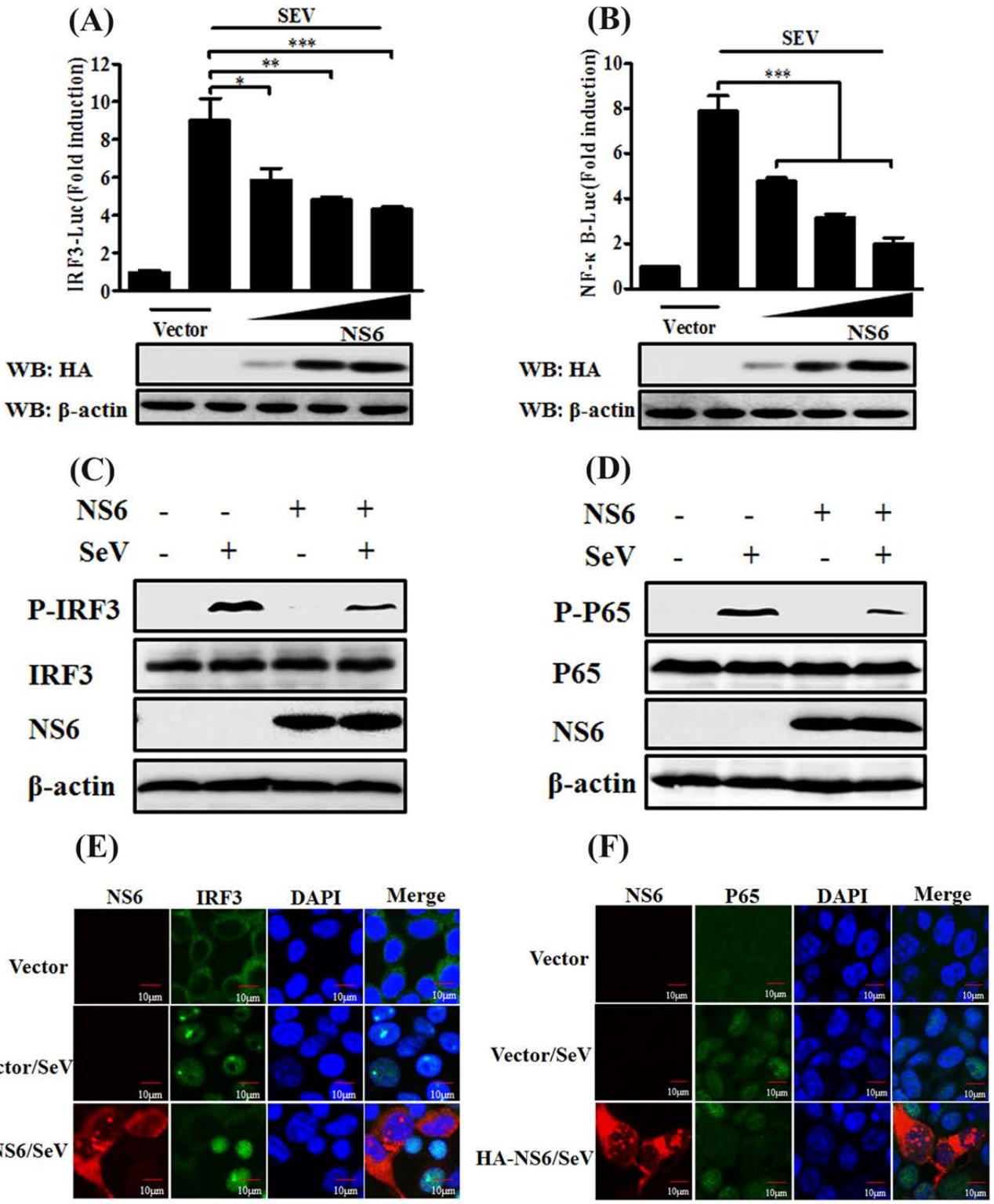

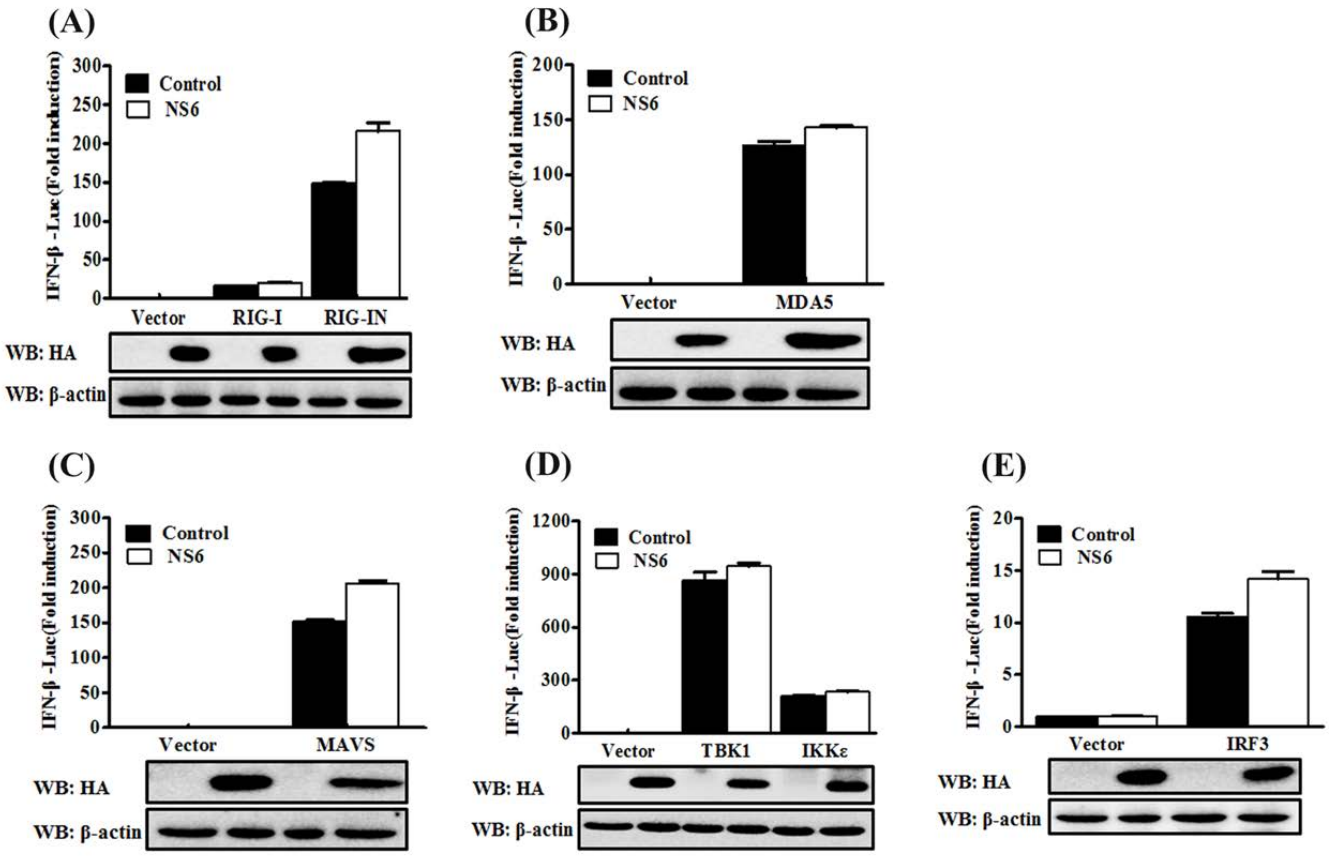

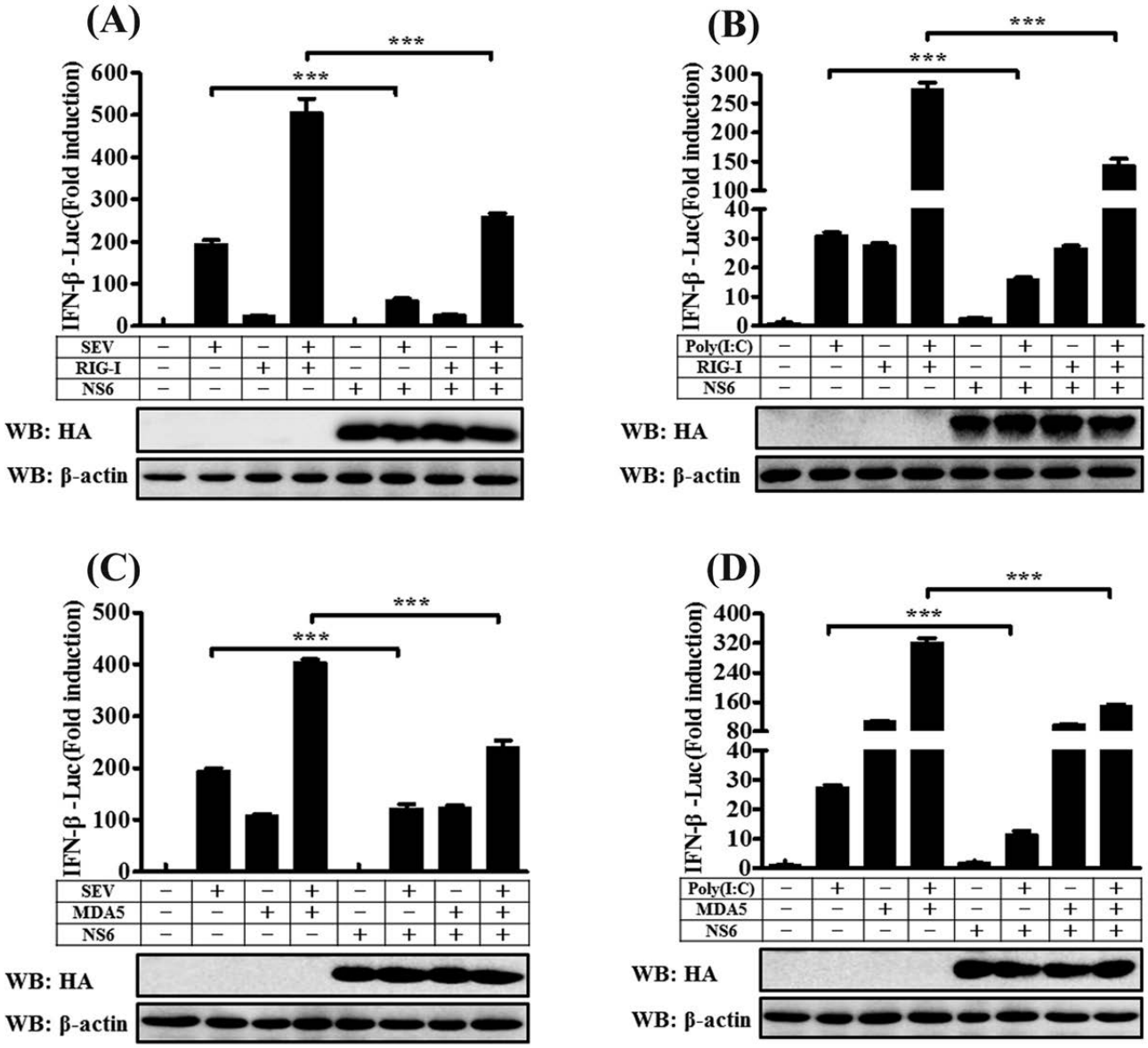

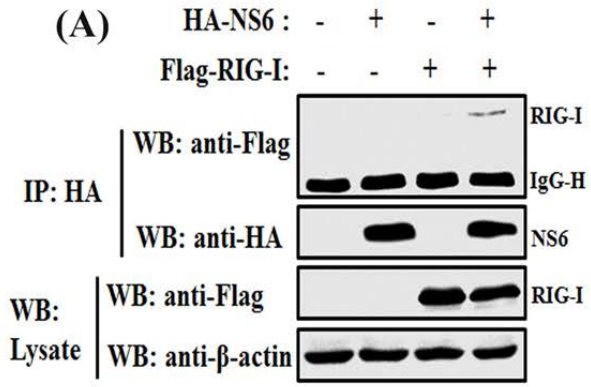

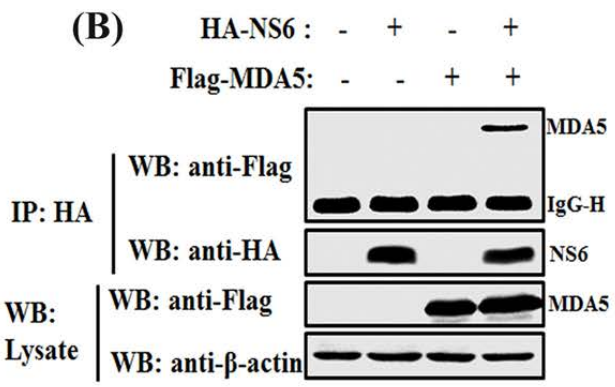

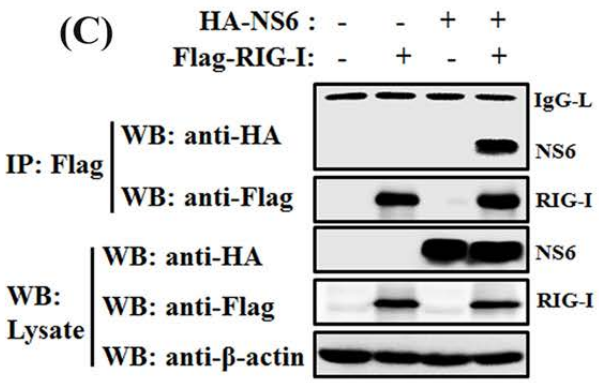

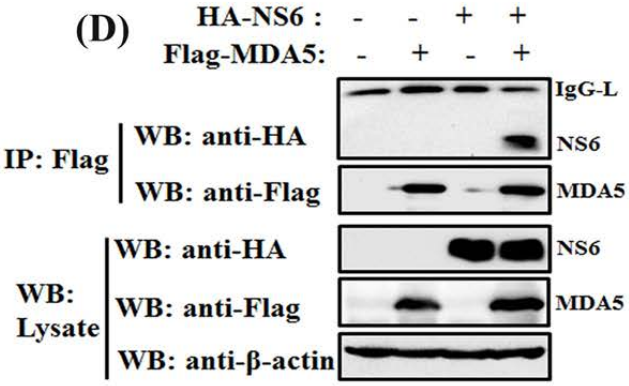

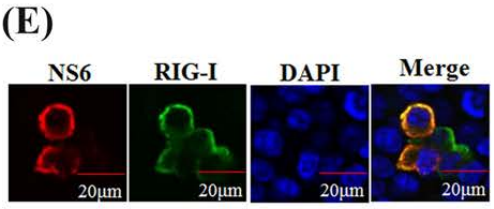

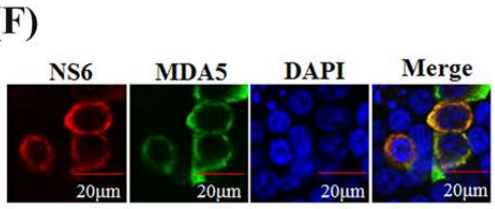

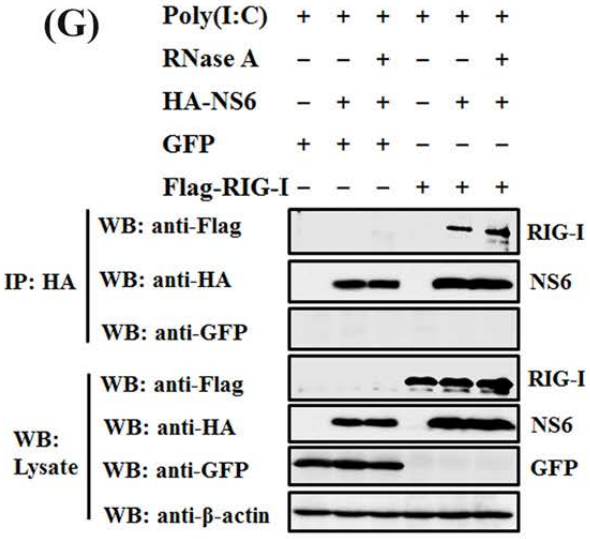

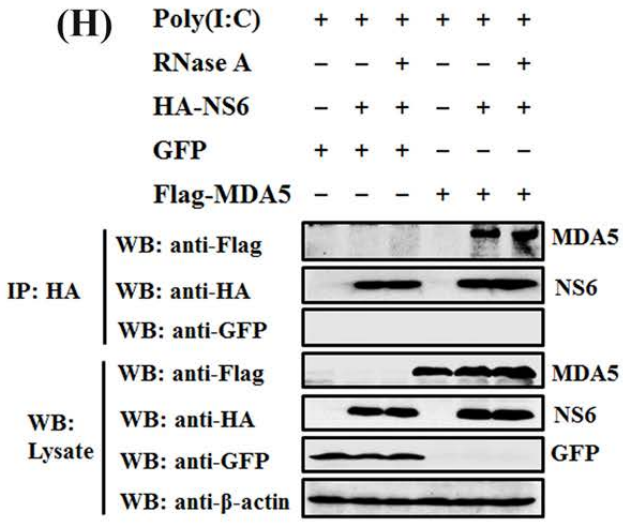

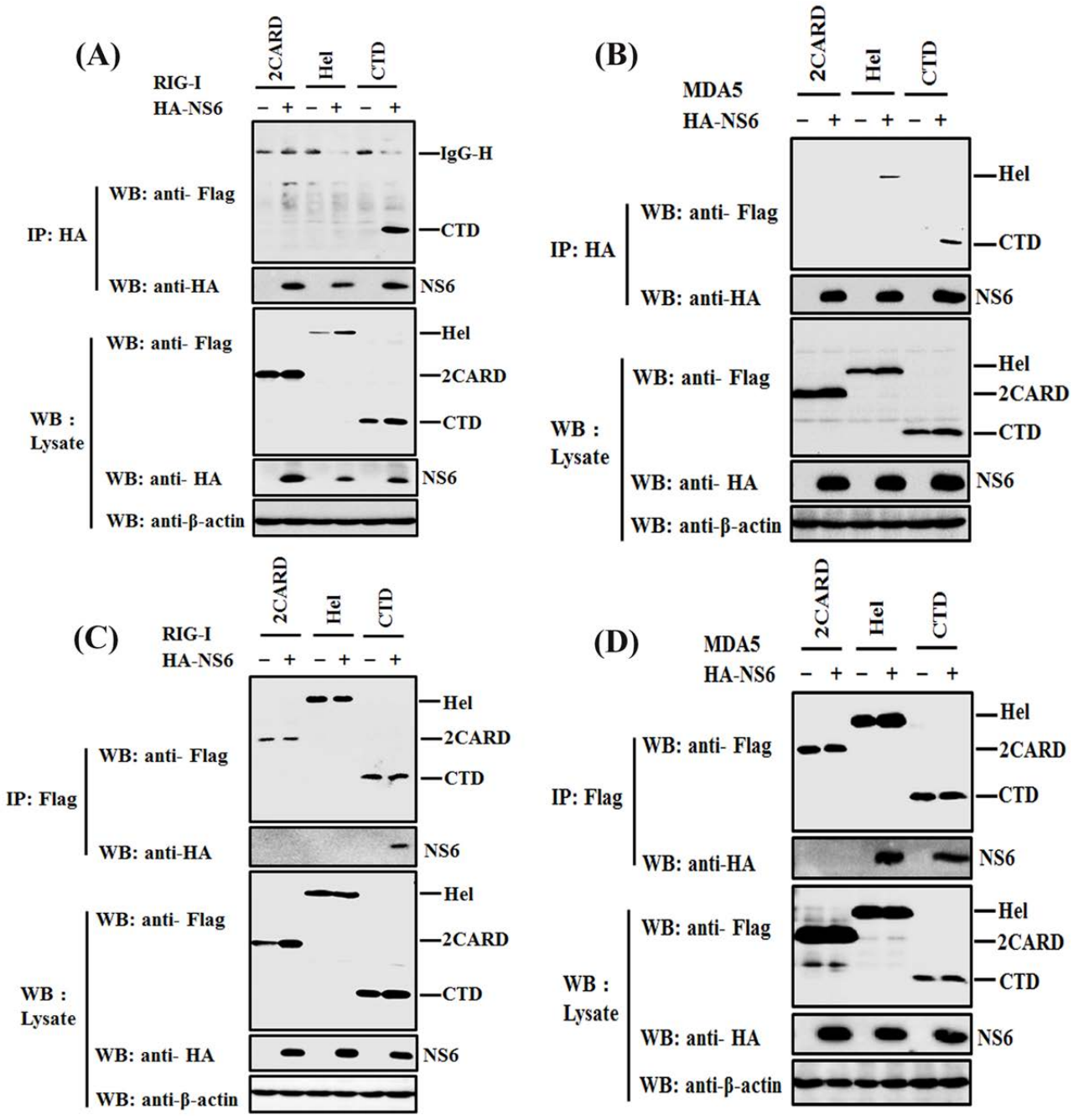

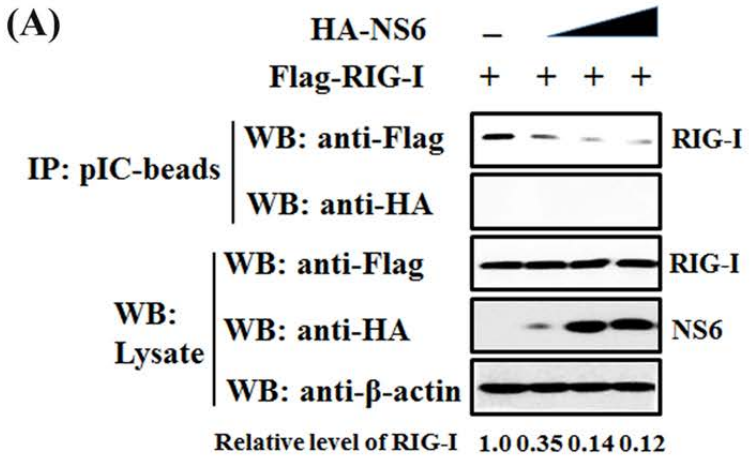

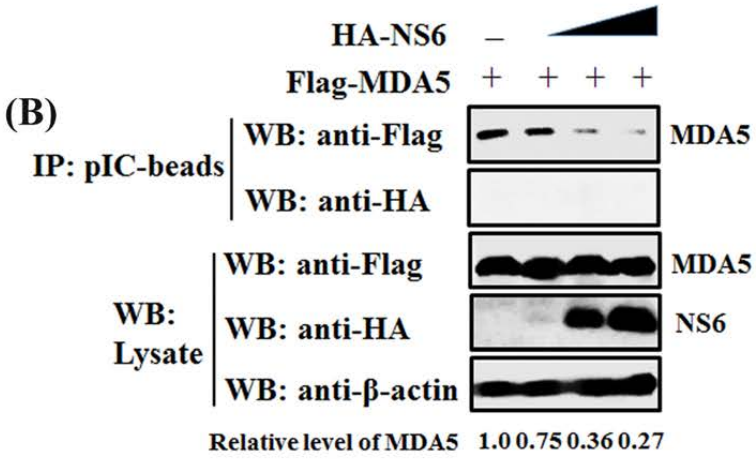

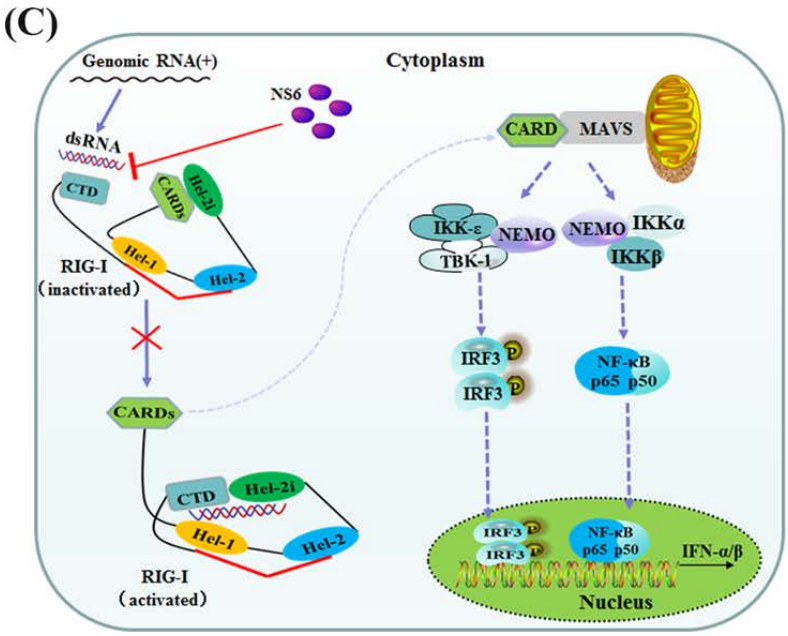

Table 1. Sequences of the primers used for real-time PCR and construction of plasmids.

Primer	Nucleotide Sequence (5'- 3')
SEV-HN-F	AAAATTACATGGCTAGGAGGGAAAC
SEV-HN-R	GTGATTGGAATGGTTGTGACTCTTA
h-GAPDH-F	TCATGACCACAGTCCATGCC
h-GAPDH-R	GGATGACCTTGCCCACAGCC
PDCoV-N-F	ACTGAATTCATGGCTGCACCAGTAGTCCCTAC
PDCoV-N-R	CTAATCGATCTACGCTGCTGATTCCTGCTTTAT
PDCoV-NS6-F	ACTGAATTCATGTGCAACTGCCATCTGCAGC
PDCoV-NS6-R	CTGCTCGAGTTAATTTAATTCATCTTCAAG
RIG-I-2CARD-F	TAAATCGATATGACCACCGAGCAGCGA
RIG-I-2CARD-R	CAGCTCGAGTCATGGACATGAATTCTC
RIG-I-Hel-F	TAAATCGATCCTTCAGAAGTGTCTGATA
RIG-I-Hel-R	CAGCTCGAGCTTATCAGGGACAGGTTTTGG
RIG-I-CTD-F	AAATCGATGAAAATAAAAAACTGCTCTG
RIG-I-CTD-R	CAGCTCGAGTCATTTGGACATTTCTGC
MDA5-2CARD-F	GCGATCGATATGTCGAATGGGTATTCCACAGAC
MDA5-2CARD-R	GCGCTCGAGTTAATTCTCTTCATCTGAATCACTTC
MDA5-Hel-F	TCTATCGATATGGTGGCAGCAAGAGCATCCCCG
MDA5-Hel-R	TATCTCGAGTTACTCATCAGCTCTGGCTCGACCA
MDA5-CTD-F	TCTATCGATATGAGCACCTACGTCCTGGTTG
MDA5-CTD-R	GCGCTCGAGCTAATCCTCATCACTAAATAAAC